

Article

Evaluation of Pilot Manipulation Comfort in Different Flight Scenarios under Different Ambient Temperatures

Xiufang Yang ^{1,2,*} , Youchao Sun ² , Zhonglin Wu ³ and Zongpeng Wang ²¹ School of Transportation Engineering, Yangzhou Polytechnic Institute, Yangzhou 225127, China² College of Civil Aviation, Nanjing University of Aeronautics and Astronautics, Nanjing 211106, China; sunyc@nuaa.edu.cn (Y.S.); wangzp@nuaa.edu.cn (Z.W.)³ Department of Basic Science, Yangzhou Polytechnic Institute, Yangzhou 225127, China; wuzhonglin_100@126.com

* Correspondence: yangxiufang654@163.com

Abstract: This study aimed to evaluate pilot manipulation comfort in different flight scenarios under different ambient temperatures. To achieve this goal, we designed a test plan to devise the physiological indexes used in the evaluation of pilot manipulation comfort, collected and analyzed pilot EMG signals and mean skin temperature, and on this basis revealed the impacts of different ambient temperatures and different flight missions on muscle activation and mean skin temperature. Based on this, we extracted muscle activation and mean skin temperature as the evaluation indices for the evaluation of manipulation comfort and established a model for this evaluation based on an improved particle swarm optimization and least-squares support vector machine (IPSO-LSSVM). Based on this model, the predicted manipulation comfort values of the participants were 4, 5 and 6, which belong to the categories of fair, somewhat comfortable and rather comfortable, respectively. By comparing the prediction results of different evaluation methods, the method proposed in this study was verified to be effective.



Citation: Yang, X.; Sun, Y.; Wu, Z.; Wang, Z. Evaluation of Pilot Manipulation Comfort in Different Flight Scenarios under Different Ambient Temperatures. *Aerospace* **2022**, *9*, 122. <https://doi.org/10.3390/aerospace9030122>

Academic Editor: Lishuai Li

Received: 5 November 2021

Accepted: 25 February 2022

Published: 28 February 2022

Publisher's Note: MDPI stays neutral with regard to jurisdictional claims in published maps and institutional affiliations.



Copyright: © 2022 by the authors. Licensee MDPI, Basel, Switzerland. This article is an open access article distributed under the terms and conditions of the Creative Commons Attribution (CC BY) license (<https://creativecommons.org/licenses/by/4.0/>).

Keywords: evaluation of manipulation comfort; muscle activation; mean skin temperature; IPSO-LSSVM; cockpit

1. Introduction

An intelligent cockpit makes it easy to steer an airplane. Some airplanes have already been equipped with touch-sensitive flight display systems. However, these systems are not yet 100% reliable. A pilot controls and manipulates an airplane. Thus, it is of great significance to study ways to improve a pilot's efficiency by enabling him or her to comfortably manipulate an aircraft in a favorable environment, thereby ensuring flight safety.

Comfort evaluation methods mainly include subjective evaluation and objective evaluation approaches. In subjective evaluation approaches [1–3], questionnaires and various comfort scales are used to evaluate the feeling of comfort for a pilot. Such evaluations are characterized by low repetitions and uncertainties. The evaluation results, which depend mainly on the pilot's subjective judgment, are prone to randomness and a large number of individual differences. In objective evaluation approaches, body pressure distribution [4,5], electrophysiological measurement, and other variables are introduced into the comfort evaluation. At present, the representative electrophysiological evaluation approaches mainly include heart rate variability (HRV) [6], electromyography (EMG) [7–10] and electroencephalography (EEG) [11]. EMG is the most widely applied method in comfort evaluation. Currently, the most commonly used noninvasive method for the objective evaluation of muscle load is the surface electromyogram (sEMG). In essence, comfort determinations are still based on the subjective experience of the operator. It requires a combination of subjective and objective characterizations of comfort, which allows for further improvement in practice [12].

In subjective and objective manipulation comfort evaluations, human–machine interactions are examined in the majority of studies [12–14]. However, the impact of environmental factors on pilot manipulation comfort has not been considered. According to the man-machine system model [15], the aircraft operation and control process involves a typical man-machine environmental control system that includes a pilot, aircraft and environment. In this situation, the pilot functions as the controller of the closed-loop system, the aircraft serves as the controlled link in the system, and the pilot operates according to the current environment. In this study, we factored in the impact of the environment on comfort based on a human–machine–environment system. Under different ambient temperatures, we collected the pilots’ myoelectric and skin temperature signals when they performed different flight missions, analyzed the changes in these signals, and used them as the input of the manipulation comfort evaluation model. The pilots’ subjective evaluations were used as the output of the model. Based on an improved particle swarm optimization and least-squares support vector machine (IPSO-LSSVM), we conducted an evaluation of pilot manipulation comfort.

2. Methodology

2.1. Evaluation Index of Manipulation Comfort

2.1.1. Muscle Activation

Muscle activation refers to the ratio of muscle stress to maximum muscle strength, which is an intuitive index for determining whether a muscle is in a comfortable or fatigued state [13]. Therefore, in the current study, we employed a surface EMG signal detection device to measure the pilot’s sEMG signal during manipulation. At the same time, we extracted muscle activation as an evaluation index for manipulation comfort.

2.1.2. Mean Skin Temperature

The temperature of the cockpit has a direct impact on the thermal comfort of a pilot, which in turn affects pilot comfort during flight manipulations. Fanger’s thermal comfort equation is widely applied in human thermal comfort evaluation standards [16]. The comfort evaluation of aircraft cockpits is based on the calculation of the predicted mean vote (PMV) indexes of the thermal comfort equation. Its shortcomings lie in the large number of parameters and complicated calculations. To find a simpler and more objective method for the thermal comfort evaluation of the human body, some researchers have introduced mean skin temperature in their studies [17], which is an index used to evaluate human thermal comfort. Therefore, we used mean skin temperature as an evaluation index for manipulation comfort.

2.1.3. Manipulation Force and Joint Torque

The manipulation force and joint torque directly affect pilot manipulation comfort. The mean manipulation force and joint torque were selected as the parameters of the manipulation comfort evaluation. In previous research, we obtained the manipulation force and the joint torque during the manipulation process, as discussed in detail in the literature [18,19].

2.1.4. Subjective Evaluation of Pilot Manipulation Comfort

The subjective evaluation of pilot manipulation comfort refers to the subjective evaluation made by the pilot according to his or her feeling of manipulation comfort when performing different flight missions in different environments. In this study, the evaluation criteria were based on the Likert psychological scale [14]. This scale divides the psychological continuum into seven fixed-choice options. The intensity of sensory changes was represented by a line segment, and points 1–7 corresponded to the intensity of sensory changes, namely: very uncomfortable, rather uncomfortable, somewhat uncomfortable, fair, somewhat comfortable, rather comfortable, and very comfortable (Figure 1). A higher score indicates a higher degree of comfort.

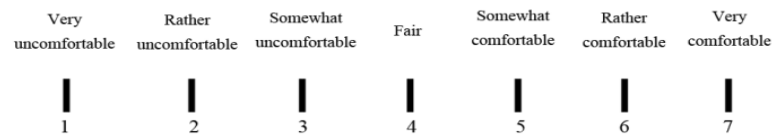


Figure 1. Evaluation criteria of the Likert scale.

Every time an operator completed a flight mission, he or she evaluated their level of manipulation comfort during the flight according to the Likert scale.

2.2. Design of the Test Plan

For typical civil aircraft flight tasks, a physiological index test for pilot control comfort was designed. Based on the semiphysical cockpit simulation control platform (15006010; Nanjing University of Aeronautics and Astronautics, Nanjing, China), by simulating different flight tasks, the physiological characteristic parameters of the pilot, such as EMG [20] and skin temperature [21], were monitored. Based on parameter analysis, we aimed to identify the mechanism underlying the influence of different ambient temperatures and different flight tasks on the physiological indexes with regard to pilot manipulation comfort.

2.2.1. Participants

Pilots with different amounts of flight experience were selected as the participants in this study. The number of participants for most tests was usually between 5–15. In this study, we selected six pilots with certain flight experience (all of them received training at Nanjing University of Aeronautics and Astronautics, Nanjing, China, received 20 months of flight training abroad and acquired a commercial pilot license) and six project researchers with a large amount of simulator experience. That is, 12 participants between 22 and 45 years old were selected for this study. Among the participants, ten were male and two were female (in real life, there are more male pilots than female pilots). The participants were required to be in good health, have good eyesight, and have no disease impeding their manipulation function. They must also have no physical pain or any psychological factors that might affect manipulation comfort. In addition, they were familiar with the operating program for the simulated flight.

2.2.2. Design of the Test Scenario

Based on the cockpit simulation control platform, the pilots were required to complete the traffic patterns (including the phases of taking off, climbing, cruising, approaching and landing), nonprecision approaches and single-engine-landing flight missions at Shanghai Hongqiao Airport at ambient temperatures of 20 °C, 26 °C, and 31 °C. The design of the test scenarios is shown in Table 1.

Table 1. Design of test scenarios.

Test Scenario	Temperature °C	Operation Task	Specific Flight Phase
1	20 °C	Takeoff and landing	Takeoff, climb, cruise, approach, and landing
2	20 °C	Nonprecision approach and single-engine landing	Descent, approach, and landing
3	26 °C	Traffic pattern	Takeoff, climb, cruise, approach, and landing
4	26 °C	Nonprecision approach and single-engine landing	Descent, approach, and landing

Table 1. *Cont.*

Test Scenario	Temperature °C	Operation Task	Specific Flight Phase
5	31 °C	Traffic pattern	Takeoff, climb, cruise, approach, and landing
6	31 °C	Nonprecision approach and single-engine landing	Descent, approach, and landing

2.2.3. Construction of the Test Platform

The human–machine–environment closed-loop simulation experiment system is shown in Figure 2. It is composed of a pilot, an aircraft simulation platform and an environment simulation cockpit, which can be used to simulate experimental ergonomics research in a specific environment.

**Figure 2.** Human–machine–environment closed-loop simulation system.

The environmental simulation cockpit is a simulation device allowing for the integration of multiple environmental factors. Table 2 shows the design indices and requirements.

Table 2. Design indexes of the environmental simulation cockpit.

Index	Requirements
Hypoxia height	0~5000 m
Noise	70~100 dB
Temperature	(5~40 °C) ± 0.2 °C
Humidity	(5~95%) ± 5%RH
Cockpit	3 × 3 × 2 = 18 m ³

A wireless physiological data acquisition and analysis system (BioNomadix; BIOPAC, Santa Barbara, CA, USA) was used to collect myoelectric signals and local skin temperature.

2.2.4. Test Procedures

- (a) Preparatory work before the experiment. Before the experiment, the participants avoided vigorous activities to prevent physical fatigue. They wore summer clothes in the simulation cockpit. After entering the environment simulation cockpit, it took approximately 20 min for the participants to adapt to their physiological conditions in the new environment.

Each pilot kept his or her chest as motionless as possible during the manipulation process. We selected five muscles as the research objects, namely, the bicep, tricep, flexor

carpi radialis, brachioradialis, and deltoid muscles. The participants' skin surface was wiped with medical alcohol, and electrode patches (LT-7; Shanghai LT Company, Shanghai, China) were pasted on. The best positions were determined by observing the EMG signal, as shown in Figure 3.

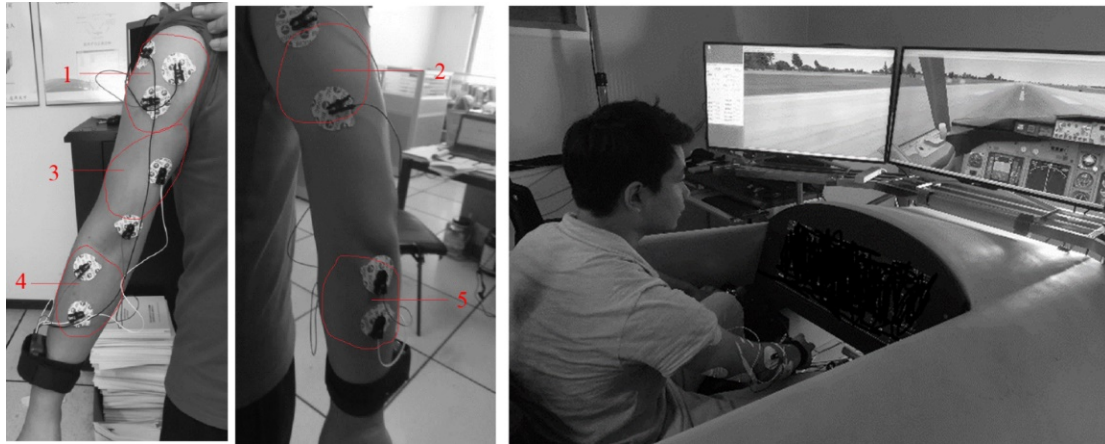


Figure 3. Schematic diagram of the locations of the upper limb muscle sEMG sensor electrode. 1. deltoid; 2. triceps; 3. biceps; 4. flexor carpi; and 5. brachioradialis.

In addition, each participant was required to participate in an experiment to test the maximum voluntary contraction (MVC) of the above five muscles before carrying out the simulated flight test. Each participant used their maximum force to pull the dynamometer and held it for 5 s in the maximum force state, during which the sEMG signal of each muscle was recorded. To prevent the subsequent experimental results from being affected by the fatigue of the muscles generated in the previous test, the participants were required to rest for at least 10 min after the maximum isometric force test before carrying out the corresponding simulated flight experiment. Otherwise, the experimental results would have been affected.

- (b) The participants assumed a comfortable sitting posture when manipulating the aircraft simulator. The designed test scenarios are shown in Table 1. All participants carried out simulated flights according to the test scenarios, and the staff collected relevant experimental data. All participants completed the subjective evaluation form with the Likert scale based on their subjective feelings after completing a test scenario. Each test scenario was repeated 5 times, and the average values of the data collected during the 5 repetitions were grouped as a set of samples. When all the participants had completed the flight operations for all the scenarios, the experiment was completed.
- (c) AcqKnowledge for Windows software (Microsoft Flight Simulator; Microsoft, Seattle, WA, USA) was used for the collation and analysis of the experimental data.

2.2.5. Collection and Processing of the Experimental Data

- (a) Acquisition and processing of EMG signals. The sEMG signal reflected the activity information of the muscle from the triggering of the muscle contraction to the end of the contraction. The voltage of the EMG signal was 0~10 mV within the signal frequency band range of 0~500 Hz. According to Shannon's sampling theorem, the frequency of the sEMG signal acquisition equipment should not be lower than 1000 Hz. Therefore, the sampling frequency was determined to be 1000 Hz.

The sEMG signal itself is relatively weak and easily affected by environmental noise. Therefore, it was necessary to clean the skin first. The skin was cleaned with an alcohol solution before the electrode patch was pasted on, as described above. After the alcohol evaporated, conductive glue was applied [22].

The sEMG signal is mainly concentrated in the 20~400 Hz range. In this study, the FIR bandpass filter (20–500 Hz) in the AcqKnowledge 4.4 software was used to filter the measured sEMG signal data to eliminate artificial signal errors caused by the movement of the surface electrode, as shown in the second and fourth rows of the figure. The adaptive option in the digital filters could also be used to filter out the noise caused by the other channels in this channel, and the filtered effect is shown in Figure 4. The first and sixth rows are the original EMG signal, and the second and fourth rows are the filtered signal. The same filter was adopted for the sEMG signal collected in the MVC experiment to ensure that the EMG signal collected in the experiment was in the same frequency domain as the EMG signal used to normalize the MVC experiment.

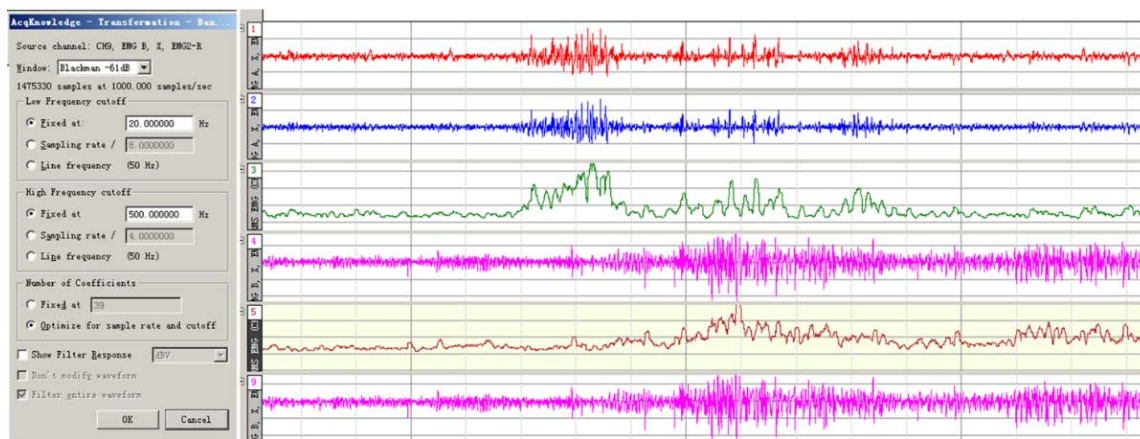


Figure 4. Comparison of the sEMG signal before and after processing. The first and sixth lines are the original EMG signal, the second and fourth lines are the filtered signal, and the third and fifth lines are the root mean square of the EMG signal.

The root-mean-square (RMS) value of the muscle sEMG signal was used to evaluate muscle activation. The 3rd and 5th rows in Figure 4 represent the RMS of the EMG signal, and the window time for the RMS calculation was 0.03 s, which is the default time in AcqKnowledge. The RMS of the sEMG signal of each operation task was normalized to 100% by MVC RMS EMG to obtain a muscle activation value in the range of [0, 1].

(b) Skin temperature signal acquisition and processing method: The BioNomadix data acquisition and analysis system was employed to measure each participant’s local skin temperature. It should be noted that, when measuring, the probe was pasted to the skin measuring point and fixed with medical tape to closely attach it to the skin.

The local skin temperatures were measured for nine parts of the human body, namely, the middle forehead, chest, nape, the middle part of the outer upper arm, the middle part of the outer forearm, the back of the hand, the middle part of the outer thigh, the middle part of the outer calf, and the back of the foot. The measuring points were all located on the left side of the participant’s body.

The calculation of mean skin temperature \bar{T}_{sk} was weighted according to nine local skin temperatures, and the calculation formula is as follows [20]:

$$\bar{T}_{sk} = 0.07T_{forehead} + 0.18T_{chest} + 0.18T_{back} + 0.07T_{upperarm} + 0.07T_{forearm} + 0.05T_{hand} + 0.19T_{thigh} + 0.13T_{calf} + 0.06T_{foot} \quad (1)$$

where $T_{forehead}$ represents the middle of the forehead, T_{chest} the chest, T_{back} the nape, $T_{upperarm}$ the middle part of the outer upper arm, $T_{forearm}$ the middle part of the outer forearm, T_{hand} the back of the hand, T_{thigh} the middle of the outer thigh, T_{calf} the middle of the outer calf, and T_{foot} the back of the foot, and different numbers indicated the weighted values of the corresponding temperatures.

3. Analysis of Results

3.1. Data Analysis of the EMG Signal

For the six test scenarios, the activations of the biceps, triceps, flexor carpi radialis, brachioradialis, and deltoid of the 12 participants are shown in Figure 5. In the same ambient environment, the activation values for the nonprecision approach and the single-engine landing missions were greater than those for the traffic pattern missions. For the nonprecision approach and the single-engine landing flight, the pilot manipulated the aircraft when one engine failed, during which time the muscle load was greater than that recorded during the traffic pattern mission. Therefore, the muscle activation values were greater. When the pilots performed the same flight mission, there were individual differences in the values of muscle activation. For example, in the sixth test scenario, among the participants, the maximum muscle activation value of the triceps was 15.75%, while the minimum value was 9.30%. Under different ambient temperatures, the activation values of most muscles exhibited a declining trend. Reference [23] noted that, when exercising in a high-temperature environment, the muscle RMS declines compared with that found in a mild environment.

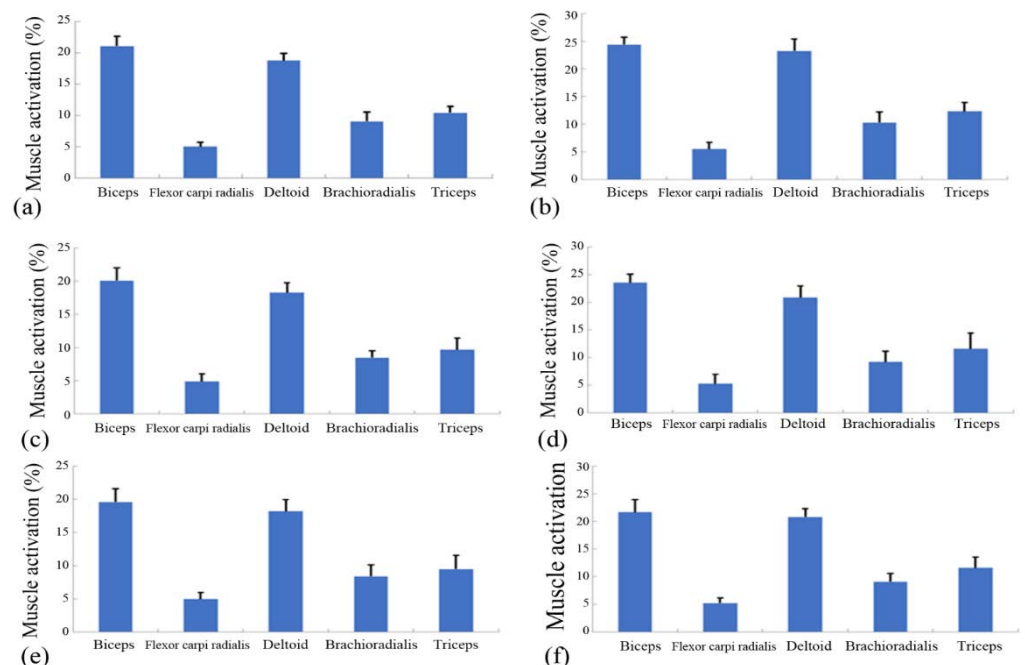


Figure 5. Muscle activation in different test scenarios. (a) Test scenario 1. (b) Test scenario 2. (c) Test scenario 3. (d) Test scenario 4. (e) Test scenario 5. (f) Test scenario 6. Abbreviations: FCR, flexor carpi radialis; and Br, brachioradialis.

In the different test scenarios, the muscle activation values of the biceps, triceps, and deltoid were greater than those of the flexor carpi radialis and the brachioradialis, as the pilot's main actions are the flexion and extension of the shoulder and elbow joints.

3.2. Data Analysis of the Skin Temperature Signal

Table 3 shows the skin temperature variations of nine test parts during different missions under different ambient temperatures. When the ambient temperature rose from 20 °C to 31 °C, the mean skin temperature of each test part gradually increased, among which the temperature of the upper limbs (upper arms, forearms, back of the hand) and lower limbs (thigh, calf, back of the foot) rose more noticeably than those of the other parts. The skin temperature of the forearm rose by approximately 5 °C when the ambient temperature rose from 20 °C to 31 °C. For the forehead, the skin temperature rose by approximately 3 °C when the ambient temperature increased from 20 °C to 31 °C. Multiple

comparisons showed that the temperatures of the local skin at different body positions exhibited significant changes with increasing environmental temperature (Table S1).

Table 3. Local skin temperature under different test scenarios.

Test Scenario	Skin Temperature (°C)								
	Forehead	Chest	Back	Upper Arm	Forearm	Hand Back	Thigh	Calf	Foot Back
1	32.98 ± 0.94	33.01 ± 1.01	32.50 ± 0.98	30.68 ± 0.92	30.11 ± 1.20	30.18 ± 1.11	30.96 ± 0.98	30.78 ± 1.05	30.58 ± 1.04
2	33.60 ± 1.23	32.96 ± 0.96	32.80 ± 0.94	31.02 ± 1.02	30.06 ± 0.89	31.02 ± 0.78	31.01 ± 1.13	30.93 ± 0.79	30.50 ± 1.05
3	34.01 ± 0.93	34.36 ± 0.77	34.22 ± 0.81	32.96 ± 0.90	32.88 ± 1.12	33.92 ± 0.99	33.32 ± 0.88	32.56 ± 0.75	33.97 ± 1.07
4	34.76 ± 0.83	34.57 ± 0.98	34.50 ± 0.69	33.25 ± 0.60	33.20 ± 0.78	34.02 ± 0.76	33.54 ± 0.83	32.99 ± 0.71	34.35 ± 0.52
5	35.33 ± 0.56	35.66 ± 0.79	35.91 ± 0.97	34.76 ± 1.01	34.89 ± 0.94	35.40 ± 0.72	34.05 ± 0.61	33.80 ± 0.70	34.74 ± 0.98
6	35.90 ± 0.61	35.96 ± 0.45	36.01 ± 0.54	35.02 ± 0.84	35.01 ± 0.96	35.80 ± 0.50	34.81 ± 0.47	34.01 ± 0.86	35.10 ± 0.66

Note: The ambient temperatures of test conditions 1–2, 3–4, and 5–6 were 20 °C, 26 °C, and 31 °C, respectively. The accuracy of this measure was 0.001 °C, but for convenience, the results here are presented in hundredths.

According to the test data in Table 3, the mean skin temperature (\bar{T}_{sk}) of the 12 participants in the 6 test scenarios was calculated to be 31.50 °C, 31.76 °C, 33.63 °C, 33.94 °C, 34.95 °C, and 35.30 °C, respectively, as shown in Figure 6.

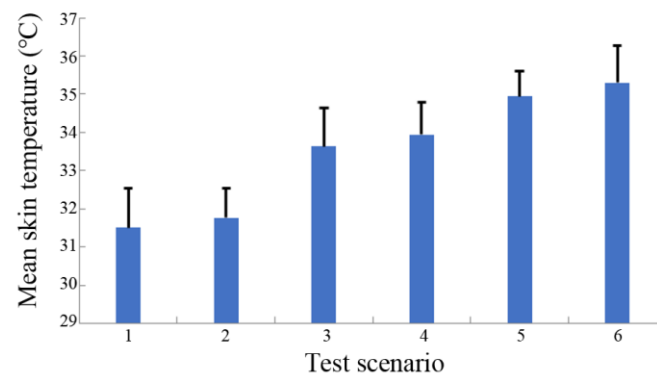


Figure 6. Mean skin temperature under different test scenarios.

It is clear from Figure 6 that, as the ambient temperature rose, the mean skin temperature rose, displaying a pattern of first larger and then smaller increases. When performing different missions, the mean skin temperature during the nonprecision approach and the single-engine-landing missions was higher than during the traffic pattern missions.

SPSS software was used to perform a multifactor analysis of variance (ANOVA) on the mean skin temperature. As shown in Table 4, for ambient temperature, $p = 0.0055 < 0.05$, indicating that the ambient temperature had a significant impact on the mean skin temperature, and for operating procedures, $p = 0.14 > 0.05$, indicating that different missions had no significant effect on the mean skin temperature.

Table 4. Analysis of variance of mean skin temperature.

Source	df	MS	F	p-Value	Fcrit
Operating procedures	1	0.18	5.81	0.14	18.51
Ambient temperature	2	5.69	179.83	0.0055	19.00

Note: A multifactor analysis of variance was performed. Abbreviations: df, degree of freedom; MS, mean square; F, statistics; and Fcrit, the critical value at the corresponding significance level.

4. Evaluation Model of Pilot Manipulation Comfort Based on IPSO-LSSVM

For traditional models, comfort evaluation is achieved through multiple linear statistical regression analysis. However, the results of the weighted average involved in these

models cannot reflect the degree of comfort well. Furthermore, the weight determination in the evaluation process is affected by human factors, which makes it difficult to accurately reflect the complex nonlinear relationship between various indicators and therefore results in a difference between the evaluation results and the actual values [12]. To date, LSSVM has been applied in the field of nonlinear prediction, which has a faster operation speed and is suitable for predicting pilot handling comfort. In this study, we constructed the LSSVM model and selected the operating force, joint torque, muscle activation and average skin temperature as the model inputs, with the subjective evaluation of handling comfort as the model output. By doing so, a combination of subjective and objective methods was used to evaluate pilot manipulation comfort.

4.1. Least-Squares Support Vector Machine

The comfort evaluation of aircraft manipulation and control is a multi-input, high-dimensional, nonlinear prediction problem. Relevance vector machines (RVMs), artificial neural networks (ANNs), and support vector machines (SVMs) are widely applied in the field of nonlinear prediction. Suykens et al. proposed the least-squares support vector machine (LSSVM) model. To compensate for the shortcomings of the standard SVM algorithm, the LSSVM algorithm is simpler in form, more convenient for solution, and faster in computation [24].

For a set of l samples (x_i, y_i) in a given area, $i = 1, \dots, l$, where $x_i \in R^s$ are some influencing factors, s is the dimension of the input vector, and y_i is the corresponding output result, the regression function of LSSVM is:

$$y = f(x) = \omega \cdot \phi(x) + b \quad (2)$$

where $\omega \in R^m$ is the weight vector and $b \in R$ is a constant representing the bias. The key problem of LSSVM is to choose a suitable mapping $\phi(x)$. The radial basis kernel function (RBF) has advantages such as a simple expression, good smoothness, radial symmetry, and a wide application range. Therefore, RBF was selected in this study. The optimization goals of LSSVM are:

$$\min J(\omega, e) = \frac{1}{2} \|\omega\|^2 + \frac{1}{2} C \sum_{i=1}^l e_i^2 \quad (3)$$

$$S.t. y_i = \omega \phi(x_i) + b + e_i, i = 1, \dots, l \quad (4)$$

where e_i is the error, $e \in R^{l \times 1}$ is the error vector, and C is the regularization parameter, whose function is to control the degree of penalty for the error.

4.2. Improved Particle Swarm Algorithm

In the iterative process of the PSO algorithm, prematurity and convergence phenomena are likely to occur. The specific measures used to improve the standard PSO algorithm in this study were as follows:

- (a) The main reason for prematurity and convergence is the lack of diversity. To address this issue, the linear decreasing strategy of the standard particle swarm algorithm was adopted. The formula is as follows:

$$\omega = \omega_{max} - (\omega_{max} - \omega_{min}) \times \frac{n}{N} \quad (5)$$

where ω_{max} and ω_{min} represent the maximum and minimum values of the inertia weight, respectively, n is the current iteration number, and N is the set maximum iteration number. Through a large number of experiments, it was proven in reference [25] that when the inertia weight ω decreased from a maximum value of 0.95 to 0.2, the local search ability and global search ability of the particle swarm were the strongest. In this study, $\omega \in [0.2, 0.95]$ was selected.

- (b) The particle distance was introduced, and the following formula was used to determine the evolution state of PSO:

$$\begin{aligned}
 d_g < \bar{d}_i & \text{ Convergent state} \\
 d_g > \bar{d}_i & \text{ Divergent state}
 \end{aligned}
 \tag{6}$$

where \bar{d}_i represents the average distance between each particle and other particles in the evolution of each generation and d_g is the average distance of the global optimal particles in the current generation. Tan [26] demonstrated that the evolution process of the PSO algorithm is unrelated to the particle speed. When the evolution of the PSO algorithm is in a convergent state, the IPSO algorithm shown in Equation (7) can fully disperse the swarm in the solution space and enhance the global search ability of the algorithm.

$$x_{in}^{k+1} = \omega \cdot x_{in}^k + c_1 \cdot rand() \cdot (p_{in} - x_{in}^k) + c_2 \cdot rand() \cdot (p_{gn} - x_{in}^k) + c_3 \cdot rand() \cdot (x_{rand} - x_{in}) \tag{7}$$

where x_{in}^{k+1} and x_{in}^k represent the $k+1$ th and k th iterations of the n th-dimension component of the position vector of particle i ; c_1 , c_2 and c_3 are the acceleration constants, which can adjust the maximum step length of learning; $rand()$ is a random function in the range $[0, 1]$, which can increase the randomness of the search; and ω is an inertia factor, which is a nonnegative number. The optimal position of the individual is denoted as $p_i = (p_{i1}, p_{i2}, \dots, p_{in})$. The optimal position of the swarm is denoted as $p_g = (p_{g1}, p_{g2}, \dots, p_{gn})$.

4.3. Evaluation Model of Pilot Manipulation Comfort

4.3.1. Selection of the Input and Output Parameters

The manipulation force, joint torque, muscle activation and mean skin temperature were used as the inputs of the pilot manipulation comfort evaluation model. The output of the model was the result of a subjective evaluation of the pilot manipulation comfort.

To unify the units of the input and output parameters, it was necessary to normalize the extracted comfort evaluation parameters. Muscle activation was reported as a percentage. The mean skin temperature and the subjective evaluation scores of manipulation comfort were normalized using Equation (8).

$$x'_i = \frac{x_i - x_{min}}{x_{max} - x_{min}} \tag{8}$$

The training samples were normalized and expressed as $\{(x_1, y_1), \dots, (x_j, y_j), \dots, (x_m, y_m)\} (j = 1, 2, \dots, m)$; then, we have:

$$x = \begin{bmatrix} x_{11} & x_{12} & x_{13} & x_{14} \\ \vdots & \vdots & \vdots & \vdots \\ x_{j1} & x_{j2} & x_{j3} & x_{j4} \\ \vdots & \vdots & \vdots & \vdots \\ x_{m1} & x_{m2} & x_{m3} & x_{m4} \end{bmatrix} Y = \begin{bmatrix} y_1 \\ \vdots \\ y_j \\ \vdots \\ y_m \end{bmatrix}$$

where Y is the sample output matrix, X is the training sample matrix, m is the number of training sample sets, x_{j1} , x_{j2} , x_{j3} , and x_{j4} represent the manipulation force, joint torque, muscle activation and mean skin temperature, respectively, and y_j is the normalized subjective evaluation score for manipulation comfort.

4.3.2. Setting of the Model Parameters

According to the research conclusions of experts and researchers [24,27], before establishing a predictive model, it is necessary to establish relevant parameters, which were:

$C \in [0.1, 150]$, $\sigma \in [0.1, 10]$, and the swarm number m , which is set artificially and can determine the calculation amount and search ability of the algorithm. Generally, the swarm number is between 20 and 40. Here, the swarm number was set to 20. The inertia weight was $\omega \in [0.2, 0.95]$, for which a linear, decreasing strategy was adopted, as shown in Equation (5). The learning factors c_1 and c_2 contributed to the learning of the particles, and after multiple summations, the particles were finally made to approach the optimal point. Usually, $c_1 = c_2 = 2$.

To further verify the superiority of the improved PSO-LSSVM, it was compared with the LSSVM and PSO-LSSVM algorithms. The settings of the other algorithm parameters are shown in Table 5.

Table 5. Settings of the algorithm parameters.

Algorithm	C	σ	m	ω	c_1	c_2
LSSVM	2	30	-	-	-	-
PSO-LSSVM	[0.1, 150]	[0.1, 10]	20	0.95	2	2
IPSO-LSSVM	[0.1, 150]	[0.1, 10]	20	[0.2, 0.95]	2	2

4.3.3. Evaluation of Manipulation Comfort

In the cockpit simulation manipulation platform, the temperature environment was set to 20 °C, 26 °C, and 31 °C, under which the pilots performed different manipulation tasks. The traffic pattern included taking off, climbing, cruising, approach and landing. During the descending phase of the nonprecision approaches and the single-engine landing missions, a fault was set on the simulator. The failure mode was single-engine failure. After setting the failure mode, the pilots were required to complete the descent, approach and landing in the single-engine failure mode. There were twelve participants in total and six test scenarios. The measured test data were divided into 72 sets, 12 of which were used as the test data of the model and 60 of which were used as the training samples of the IPSO-LSSVM model. A simulation analysis was conducted based on the MATLAB 2015b platform. The prediction results are shown in Table 6. In this table, participants no. 1 to no. 6 were experienced pilots, and the remaining were researchers with a large amount of simulator experience. As shown in the table, the absolute errors for these participants were all small. The actual values of the two female participants (no. 10 and no. 11) were 3.89 and 3.95, respectively, which belonged to the category of fair comfort, and those of the male participants fell in the categories of being somewhat comfortable and rather comfortable.

Table 6. Prediction results of the IPSO-LSSVM model.

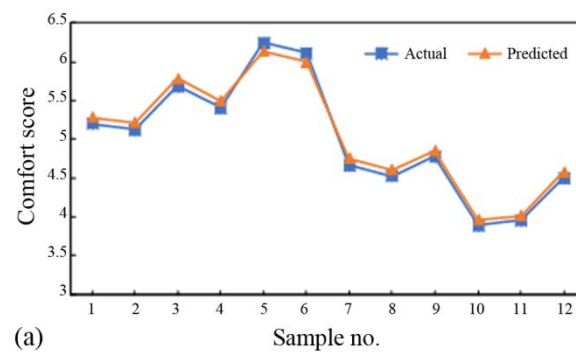
Serial Number	Actual Value	Predicted Value	Absolute Error
1	5.20	5.28	0.08
2	5.12	5.21	0.09
3	5.68	5.78	0.10
4	5.40	5.49	0.09
5	6.24	6.14	0.10
6	6.11	6.00	0.11
7	4.66	4.75	0.09
8	4.52	4.6	0.08
9	4.78	4.85	0.07

Table 6. *Cont.*

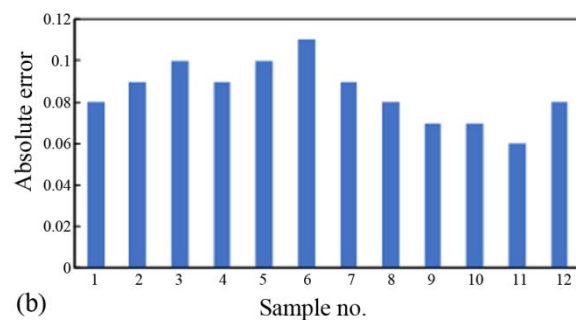
Serial Number	Actual Value	Predicted Value	Absolute Error
10 *	3.89	3.96	0.07
11 *	3.95	4.01	0.06
12	4.50	4.58	0.08

* Note: No. 1–no. 6 were experienced pilots. No. 7–no. 12 were researchers with a large amount of simulator experience. No. 10 and no. 11 were female.

Figure 7a shows the prediction results, and Figure 7b shows the absolute error. The prediction effect of this model was good, with an absolute error between 0.06 and 0.11.



(a)



(b)

Figure 7. Prediction results of the IPSO-LSSVM algorithm. (a) Comparison of the actual values and predicted values. (b) Absolute error.

To verify the accuracy of the IPSO-LSSVM algorithm, the prediction results for LSSVM, PSO-LSSVM and IPSO-LSSVM were compared. The absolute error results are shown in Figure 8.

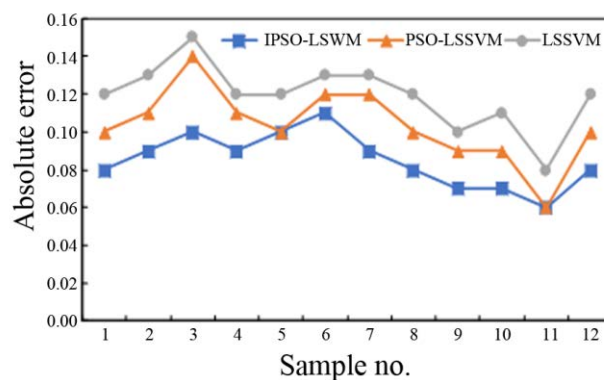


Figure 8. Absolute error results of different models.

To facilitate the evaluation of the accuracy of each algorithm, the root-mean-square error (RMSE) and the mean absolute percentage error (MAPE) were used for comparative analysis, as shown in Equations (9) and (10).

$$RMSE = \sqrt{\frac{\sum_{i=1}^n (y_{pi} - y_{si})^2}{n}} \quad (9)$$

$$MAPE = \frac{\sum_{i=1}^n \left| \frac{y_{pi} - y_{si}}{y_{si}} \right|}{n} \times 100\% \quad (10)$$

where y_{si} is the actual value and y_{pi} is the predicted value.

As calculated by Equations (9) and (10), the evaluation results of the different algorithms are shown in Table 7.

Table 7. Comparison of the evaluation results of different algorithms.

Model	RMSE	MAPE (%)
LSSVM	0.120	2.37
PSO-LSSVM	0.105	2.05
IPSO-LSSVM	0.086	1.68

The comparison results show that the RMSE and MAPE values of IPSO-LSSVM were smaller than those of LSSVM and PSO-LSSVM, demonstrating that this model had a higher prediction accuracy. Among them, the RMSE values of IPSO-LSSVM were 0.034 and 0.019 less than those of LSSVM and PSO-LSSVM, respectively. The MAPE value of IPSO-LSSVM was smaller than those of LSSVM and PSO-LSSVM by 0.69 and 0.37 percentage points, respectively. The above results show that the IPSO-LSSVM model yields better performance in evaluating pilot manipulation comfort.

5. Conclusions

The summary of this study is as follows:

- (1) In this study, we designed a test plan for the physiological indexes used to evaluate pilot comfort in manipulating aircraft, and collected and analyzed the pilot electromyographic signal, mean skin temperature, and biceps, triceps, flexor carpi radialis, brachioradialis, and deltoid activation of the 12 participants. Under the same temperature environment, the nonprecision approach and single-engine landing missions exhibited greater muscle activation values than the traffic pattern flight missions. Under different ambient temperatures, the activation values of most muscles showed a declining trend. When the ambient temperature rose from 20 °C to 31 °C, the mean skin temperature of nine test locations on the participants gradually increased, among which the temperature of the upper limbs (upper arm, forearm, and back of hand) and lower limbs (thigh, calf, and back of foot) rose more significantly than that of the other parts. Under different missions, the mean skin temperature during the nonprecision approach and the single-engine landing was higher than that during the traffic pattern missions.
- (2) We also constructed a pilot comfort evaluation model based on IPSO-LSSVM and selected the manipulation force, joint torque, muscle activation and mean skin temperature as the inputs of the model and the subjective evaluation results of the manipulation as the output of the model. Sixty sets of data were used as the training samples of the IPSO-LSSVM model, and 12 sets of data were used as the test data of the model. Based on the MATLAB 2015b platform, we predicted the manipulation comfort evaluation. Using the parameters RMSE and MAPE, we compared the

three algorithms, namely LSSVM, PSO-LSSVM and IPSO-LSSVM, demonstrating that the prediction accuracy of the IPSO-LSSVM method was higher. Based on the human–machine–environment system, we evaluated pilot manipulation comfort by combining subjective and objective methods, shedding light on the evaluation of pilot manipulation comfort.

This study suffers from some limitations. First, the sample size of this study was small. Future studies with a larger sample size will be conducted to validate the results of this study. Second, the proportion of female participants was small, which might cause bias in the results obtained in this study. Although our results did not show that the model proposed in this study was applicable to both male and female operators, future studies with a more balanced ratio of male to female operators should also be conducted.

Currently, the evaluation methods for pilot comfort in a civil flight include subjective methods, such as the Cooper–Harper Handling Qualities Rating Scale and the NASA TLX Likert psychological scale, and objective methods, such as electrocardiography, electromyography (EMG) and electroencephalograms, and the EMG method is the most frequently employed evaluation method. In this study, we combined the pilot’s subjective evaluation (the Likert scale) with objective evaluations (EMG and skin temperature) to assess pilot comfort degree, which is expected to enhance flight safety in the future. Based on this study, the factor of the cockpit vibrational environment can be integrated into the model to investigate the influence of this factor on pilot manipulation comfort. If experimental conditions are permitted, the operating environment with different vibration intensities and excitation frequencies can be taken into account to collect the sEMG signals of the pilot’s main muscles for manipulation comfort assessment.

Supplementary Materials: The following supporting information can be downloaded at: <https://www.mdpi.com/article/10.3390/aerospace9030122/s1>. Table S1: Multiple pairwise comparisons of the changes in the temperature of the skins at different positions according to environmental temperature.

Author Contributions: Conceptualization, X.Y.; methodology, Y.S.; software, Z.W. (Zhonglin Wu); validation, Z.W. (Zongpeng Wang); formal analysis, Z.W. (Zhonglin Wu); investigation, X.Y. and Z.W. (Zhonglin Wu); resources, Y.S.; data curation, Z.W. (Zhonglin Wu); writing—original draft preparation, X.Y.; writing—review and editing, Y.S.; visualization, Z.W. (Zongpeng Wang); supervision, Y.S.; project administration, Y.S.; funding acquisition, Y.S. All authors have read and agreed to the published version of the manuscript.

Funding: This work is supported by the Joint Fund of the National Natural Science Foundation of China and Civil Aviation Administration of China (Nos. U2033202 and U1333119) and the National Natural Science Foundation of China (No. 52172387).

Institutional Review Board Statement: Not applicable.

Informed Consent Statement: Not applicable.

Data Availability Statement: The data analyzed in this study are available within the article and supplementary table.

Conflicts of Interest: The authors declare no conflict of interest. The funders had no role in the design of the study; in the collection, analyses, or interpretation of data; in the writing of the manuscript; or in the decision to publish the results.

References

1. Tamura, K.; Matsumoto, S.; Tseng, Y.H.; Kobayashi, T.; Miwa, J.I.; Miyazawa, K.I.; Hirao, T.; Hiramatsu, S.; Otake, H.; Okamoto, T. Physiological and subjective comfort evaluation under different airflow directions in a cooling environment. *PLoS ONE* **2021**, *16*, e0249235. [[CrossRef](#)] [[PubMed](#)]
2. Rubio, S.; Díaz, E.; Martín, J.; Puente, J.M. Evaluation of subjective mental workload: A comparison of SWAT, NASA-TLX, and workload profile methods. *Appl. Psychol.* **2004**, *53*, 61–86. [[CrossRef](#)]
3. Smith, D.R.; Andrews, D.M.; Wawrow, P.T. Development and evaluation of the automotive seating discomfort questionnaire (ASDQ). *Int. J. Ind. Ergon.* **2006**, *36*, 141–149. [[CrossRef](#)]

4. Milivojevic, A.; Stanciu, R.; Russ, A.; Blair, G.R.; Heumen, J.D. *Investigating Psychometric and Body Pressure Distribution Responses to Automotive Seating Comfort*; SAE Technical Paper 2000-01-0626; SAE International: Warrendale, PA, USA, 2000. [[CrossRef](#)]
5. Winkleby, M.A.; Ragland, D.R.; Fisher, J.M.; Syme, S.L. Excess risk of sickness and disease in bus drivers: A review and synthesis of epidemiological studies. *Int. J. Epidemiol.* **1988**, *17*, 255–262. [[CrossRef](#)] [[PubMed](#)]
6. Ikeda, K.; Endo, A.; Minowa, R.; Narita, T.; Kato, H. Ride comfort control system considering physiological and psychological characteristics: Effect of masking on vertical vibration on passengers. *Actuators* **2018**, *7*, 42. [[CrossRef](#)]
7. Ospina-Mateus, H.; Jiménez, L.A.Q. Understanding the impact of physical fatigue and postural comfort experienced during motorcycling: A systematic review. *J. Transp. Health* **2019**, *12*, 290–318. [[CrossRef](#)]
8. Trask, C.; Teschke, K.; Morrison, J.; Johnson, P.; Village, J.; Koehoorn, M. EMG estimated mean peak and cumulative spinal compression of workers in five heavy industries. *Int. J. Ind. Ergon.* **2010**, *40*, 448–454. [[CrossRef](#)]
9. Ryait, H.S.; Arora, A.S.; Agarwal, R. Interpretations of wrist/grip operations from SEMG signals at different locations on arm. *IEEE Trans. Biomed. Circuits Syst.* **2010**, *4*, 101–111. [[CrossRef](#)] [[PubMed](#)]
10. Wang, Y.; Liu, Y.; Xu, M.W. Fatigue test of workers upper limb muscle Fatigue based on Electromyography. *J. North China Inst. Sci. Technol.* **2019**, *16*, 98–102.
11. Guan, H.; Hu, S.; Lu, M.; He, M.; Liu, G. Analysis of human electroencephalogram features in different indoor environments. *Build. Environ.* **2020**, *186*, 107328. [[CrossRef](#)]
12. Hu, J.; Qian, P.; Liu, M.Z.; Zhang, M.; Zheng, D. Human-machine interaction manipulation comfort evaluations based on muscle physiological signals. *China Mech. Eng.* **2018**, *29*, 200–204.
13. Rosaria, C.; Alessandro, N.; Chiara, C. Comfort seat design: Thermal sensitivity of human back and buttock. *Int. J. Ind. Ergon.* **2020**, *78*, 102961. [[CrossRef](#)]
14. Meng, J. *Driver Lumbar Comfort Research Based on Musculoskeletal Biomechanical Loadings*. Ph.D. Thesis, Tsinghua University, Beijing, China, 2015.
15. Ryutase, C. *Automotive Ergonomics*; Machinery Industry Press: Beijing, China, 2018.
16. Hei, S.G.; Jiang, S.G.; Yang, J.; Zhang, J.L. The development process and applicability analysis of Fanger PMV thermal comfort model. *Low Temp. Archit. Technol.* **2017**, *39*, 125–128.
17. Humphreys, M.A.; Mc Cartney, K.J.; Nicol, J.F. An analysis of some observations of the finger temperature and thermal comfort of office workers. *Proc. Indoor Air* **1999**, *1999*, 602–607.
18. Yang, X.F.; Sun, Y.C.; Zhao, D.X.; Guo, Y.D.; Tang, B. Analysis of pilot manipulation comfort based on screw kinematic model. *Mach. Tool Hydraul.* **2018**, *46*, 27–35.
19. Yang, X.F.; Sun, Y.C.; Zhao, D.X.; Yang, Z.D.; Yao, L.J.; Guo, Y.D. Dynamics analysis of pilot's upper limb manipulation process. *J. Adv. Mech. Des. Syst. Manuf.* **2018**, *12*, JAMDSM0119. [[CrossRef](#)]
20. Wheeler, K.R. Device Control Using Gestures Sensed from EMG SMCia. In Proceedings of the IEEE International Workshop on Soft Computing in Industrial Applications, Binghamton, NY, USA, 25–25 June 2003.
21. Yang, Z.Z. *The Research of Thermal Comfort for Human in Spaceflight*; The Fourth Military Medical University: Xi'an, China, 2014.
22. Liang, P.D. *Research on Man-Machine Action Information Transmission Based on Surface EMG Signals*. Ph.D. Thesis, Harbin University of Technology, Haerbin, China, 2017.
23. Yang, G.S. Effects of high temperature and high humidity on the fatigue of athletes in general environmental endurance exercise and related mechanisms. *J. Xi'an Jiaotong Univ.* **2019**, *40*, 664–669.
24. Xiong, Y.H. *Design and Implementation of Short-Term Load Forecasting System Based on Improved PSO-LSSVM*. Ph.D. Thesis, Anhui University, Hefei, China, 2019.
25. Suganthan, P.N. Particle Swarm Optimiser with Neighborhood Operator. In Proceedings of the Congress on Evolutionary Computation, Washington, DC, USA, 6–9 July 1999; pp. 1958–1962.
26. Tan, L. A Clustering K-Means Algorithm Based on Improved PSO Algorithm. In Proceedings of the Fifth International Conference on Communication Systems and Network Technologies, Gwalior, India, 4–6 April 2015; pp. 940–944.
27. Ma, H.F. *Research and Application of Short-Term Power Load Forecasting Based on Support Vector Machine*; Lanzhou University of Technology: Lanzhou, China, 2018.